Surface Enhanced Second Harmonic Generation from Macrocycle, Catenane, and Rotaxane Thin Films: Experiments and Theory

Imad Arfaoui,[†] Verónica Bermúdez,[‡] Giovanni Bottari,[§] Celine De Nadai,[⊥] Jukka-Pekka Jalkanen,[||] François Kajzar,[‡,†] David A. Leigh,*[,§] Monika Lubomska,[†] Sandra M. Mendoza,[†] Jacek Niziol,[‡] Petra Rudolf,*[,†] and Francesco Zerbetto*[,||]

Materials Science Centre, University of Groningen, Nijenborgh 4, NL-9747 AG Groningen, The Netherlands, Commissariat à l'Energie Atomique, DRT-LITEN, DSEN/GENEC/L2C, CEA/Saclay, F-91191 Gif sur Yvette, France, School of Chemistry, University of Edinburgh, The King's Buildings, West Mains Road, Edinburgh EH9 3JJ, United Kingdom, Laboratoire Interdisciplinaire de Spectroscopie Electronique, Facultés Universitaires Notre-Dame de la Paix, 61 rue de Bruxelles, B-5000 Namur, Belgium, and Dipartimento di Chimica "G. Ciamician", Università di Bologna, via F. Selmi 2 I-40126 Bologna, Italy

Received: October 26, 2005; In Final Form: February 24, 2006

Surface enhanced second harmonic generation (SE SHG) experiments on molecular structures, macrocycles, catenanes, and rotaxanes, deposited as monolayers and multilayers by vacuum sublimation on silver, are reported. The measurements show that the molecules form ordered thin films, where the highest degree of order is observed in the case of macrocycle monolayers and the lowest in the case of rotaxane multilayers. The second harmonic generation activity is interpreted in terms of electric field induced second harmonic (EFISH) generation where the electric field is created by the substrate silver atoms. The measured second order nonlinear optical susceptibility for a rotaxane thin film is compared with that obtained by considering only EFISH contribution to SHG intensity. The electric field on the surface of a silver layer is calculated by using the Delphi4 program for structures obtained with TINKER molecular mechanics/dynamics simulations. An excellent agreement is observed between the calculated and the measured SHG susceptibilities.

1. Introduction

Catenanes and rotaxanes are mechanically interlocked molecules composed of moving parts.[1−3] They are organic systems which offer unique architectural and structural properties and have attracted great attention as promising candidates for applications in photonics, particularly in all optical and electrooptical switching.[4] The catenanes are formed by interlocking two or more macrocycles. In the case of rotaxanes, one or more macrocycles are locked onto a thread by two bulky stoppers located at both ends of the thread (e.g., two phenyl rings in fumaramide [2]rotaxane). The macrocycles can move (shuttle) or circumrotate around a thread and the shuttling movement is limited by the stoppers.[5,6]

Large catenanes (MW $>10^5$) are found in nature, e.g., in DNA as intermediates during the replication, transcription, and recombination process.[7] Since the first two-ring catenane was obtained in the early sixties,[8] smaller synthetic catenanes (MW $= 10^3$) have attracted the interest of chemists and physicists. Both catenanes and rotaxanes can be functionalized and their physicochemical properties can be tailored by derivatization. They can also be processed into good optical quality thin films by vacuum sublimation.[4] The linear and nonlinear optical properties of these films were studied by various techniques and the results of these investigations are presented and discussed in this report. An emphasis is put on Surface Enhanced Second Harmonic Generation (SE SHG) experiments, which combined with theoretical calculations lead to molecular orientation determination and a better understanding of the system.

2. Experimental Details

The synthesis of the benzylic amide macrocycle (1,7,14,20-tetraaza-2,6,15,19-tetraoxo-3,5,9,12,16,18,22,25-tetrabenzocyclohexosane), benzylic amide [2]catenane (1,7,14,20-tetraaza-2,6,15,19-tetraoxo-3,5,9,12,16,18,22,25-tetrabenzocyclohexacosane)-(1′,7′,14′,20′-tetraaza-2′,6′,15′,19′-tetraoxo-3′,5′,9′,12′,16′,18′,22′,25′-tetrabenzocyclohexacosane), and the fumaramide [2]rotaxane ([2]-(1,7,14,20-tetraaza-2,6,15,19-tetraoxo-3,5,9,12,16,18,22,25-tetrabenzocyclohexacosane)-(*E*)-(*N*,*N*′-bis(2′,2′-diphenylethyl)-2′-butanediamide)rotaxane) studied in this work are described elsewhere.[9−13] For simplicity, we will refer to them in the text as benzylic amide macrocycle, benzylic amide catenane, and fumaramide [2]rotaxane or just as macrocycle, catenane, and rotaxane, respectively. Figure 1 shows schematic drawings of the chemical structure of these three compounds.

For the study of ordering by SE SHG, thin films of catenane, rotaxane, and macrocycle were prepared by high vacuum (HV) sublimation (10^{-7} Torr) onto polycrystalline Ag substrates. Ag substrates were obtained by vacuum sublimation onto freshly cleaved mica to yield nontransparent layers of 400 nm thickness. Prior to depositing the organic molecules, the Ag films were cleaned in situ by cycles of argon ion bombardment until

* Corresponding author for SHG experiments: François Kajzar. E-mail: Francois.KAJZAR@cea.fr. Corresponding author for sample preparation/characterization: Petra Rudolf. E-mail: p.rudolf@rug.nl. Corresponding author for theoretical calculations: Francesco Zerbetto. E-mail: francesco.zerbetto@unibo.it. Corresponding author for materials: David Leigh. E-mail: david.Leigh@ed.ac.uk.

[†] University of Groningen.

[‡] Commissariat à l'Energie Atomique.

[§] University of Edinburgh.

[⊥] Facultés Universitaires Notre-Dame de la Paix.

[||] Università di Bologna.

10.1021/jp0561468 CCC: $30.25
Published on Web 03/30/2006

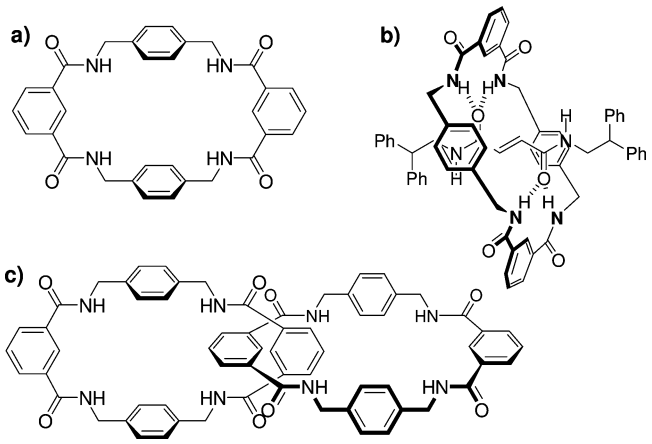

Figure 1. Schematic representation of (a) benzylic amide macrocycle; (b) fumaramide [2]rotaxane, composed of a macrocycle locked onto a thread by two bulky stoppers; and (c) benzylic amide [2]catenane, composed of two identical interlocked macrocycles.

no contaminants could be detected by high-resolution electron energy loss spectroscopy (HREELS) or X-ray photoelectron spectroscopy (XPS).

The organic molecules were sublimed in an ultrahigh vacuum (UHV) system (base pressure of 2×10^{-10} Torr) onto the substrates kept at 300 K with use of a custom built cell that consisted of a Pyrex crucible topped with a 2 mm stainless steel collimator. The crucible was heated resistively to 500 K for benzylic amide macrocycle and 470 K for benzylic amide [2]-catenane and fumaramide [2]rotaxane with the temperature being measured by a chromel−alumel junction fixed at the tube exit. Exposures were monitored with an uncalibrated Bayard-Alpert ionization gauge. The film thickness was 137 Å for the catenane film, 1073 Å for the macrocycle film, both measured with a profilometer, and ∼100 Å for the rotaxane film, measured by Atomic Force Microscopy. The molecular thin films were characterized by HREELS or XPS in situ in the UHV system to check the cleanliness and verify that the layers showed bulklike characteristics, i.e., a very strong attenuation of the substrate photoemission peaks, no interface components in the C1s and N1s photoemission spectra and/or HREELS spectra without a Au−O stretching mode, the latter being normally observed only for coverage up to the monolayer.[14−16] To prepare a monolayer film of either macrocycle, catenane, and rotaxane, bulklike films were annealed in situ to induce desorption of all molecules not chemisorbed to the Ag substrate. In the case of macrocycle and catenane, the characteristic monolayer spectrum was identified by HREELS after this treatment.[14−16] With these references, spectra corresponding to less than or more than a monolayer can be identified with confidence. In a similar way we determined by XPS that rotaxane sublimes intact and the monolayer coverage can be obtained by selective desorption of the multilayer.[17]

The optical measurements were performed with a Q switched Nd:YAG laser, operating at a fundamental wavelength of 1064 nm, with an operation rate of 10 pps and a pulse duration of 13 ns. The experiments were carried out in reflection geometry. The sample and a dichroic mirror, reflecting the harmonic at 532 nm wavelength, were mounted on rotation stages. Both rotations were synchronized. The direction of the polarization of the incident wave was varied continuously by rotating a half-wave plate at the fundamental wavelength. The harmonic beam polarization was checked with a Glan-Thomson polarizer at a fixed direction during the experiments.

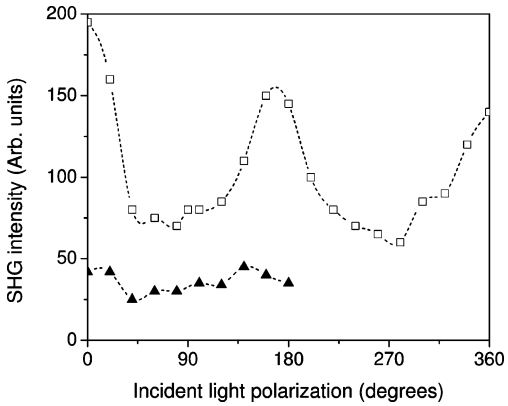

Figure 2. Fundamental beam polarization dependence of SHG intensity from a monolayer of fumaramide [2]rotaxane on Ag(111) (□) and from the silver surface alone (▲). The harmonic beam polarization is of p-type.

3. Results and Discussion

3.1. Surface Enhanced Second Harmonic Generation Experiments. Figure 2 shows harmonic fields detected from a rotaxane monolayer on silver and from the silver surface alone. The angles 0° and 180° correspond to p-type polarization of the fundamental beam. The harmonic polarization is fixed to be p-type. A small signal from the silver layer is detected, which is significantly weaker than the one coming from the monolayer. For the rotaxane monolayer we observe a strong dependence of SHG intensity on the fundamental beam polarization direction. This behavior is typical for poled thin films and characterized by two nonzero $\chi^{(2)}(-2\omega;\omega,\omega)$ tensor components: $\chi^{(2)}_{sp}$ and $\chi^{(2)}_{pp}$. It corresponds to the thin film symmetry ∞mm, with the rotation axis perpendicular to the thin film substrate. Both susceptibilities are expressed by configurational averages, assuming (for the sake of simplicity) that there is only one nonzero first hyperpolarizability β component, β_{zzz}:

$$\chi^{(2)}_{pp}(-2\omega;\omega,\omega) = NF\beta_{zzz}(-2\omega;\omega,\omega)\langle\cos^3\Theta\rangle \qquad (1)$$

and

$$\chi^{(2)}_{sp}(-2\omega;\omega,\omega) = \frac{1}{2}NF\beta_{zzz}(-2\omega;\omega,\omega)\langle\sin^2\Theta\cos\Theta\rangle \qquad (2)$$

where N is the density of molecules, F is the local field factor, and Θ is the angle between the symmetry axis and the probing optical field direction. Thus, the ratio of the two nonzero $\chi^{(2)}$ tensor components

$$a = \frac{\chi^{(2)}_{pp}(-2\omega;\omega,\omega)}{\chi^{(2)}_{sp}(-2\omega;\omega,\omega)} \qquad (3)$$

is a measure of the order and takes values between 1 and ∞.

Although the exact value of β_{zzz} (eqs 1−2) has no infuence on the order parameter a (cf. eq 3) we suppose, as it will be shown later, that it is dominated by the electric field induced (EFISH) component $\gamma(-2\omega;\omega,\omega,0)E$, where E is the electric field perpendicular to the silver surface and $\gamma(-2\omega;\omega,\omega,0)$ is the second molecular EFISH hyperpolarizability. As all studied molecules are almost centrosymmetric the "proper" molecular first hyperpolarizability of studied molecules β is expected to be negligible and most likely of quadrupolar origin. As the $\gamma(-2\omega;\omega,\omega,0)$ hyperpolarizability depends strongly on the number of π electrons, it is expected that β_{zzz} will be largest for the rotaxane and smallest for the macrocycle.

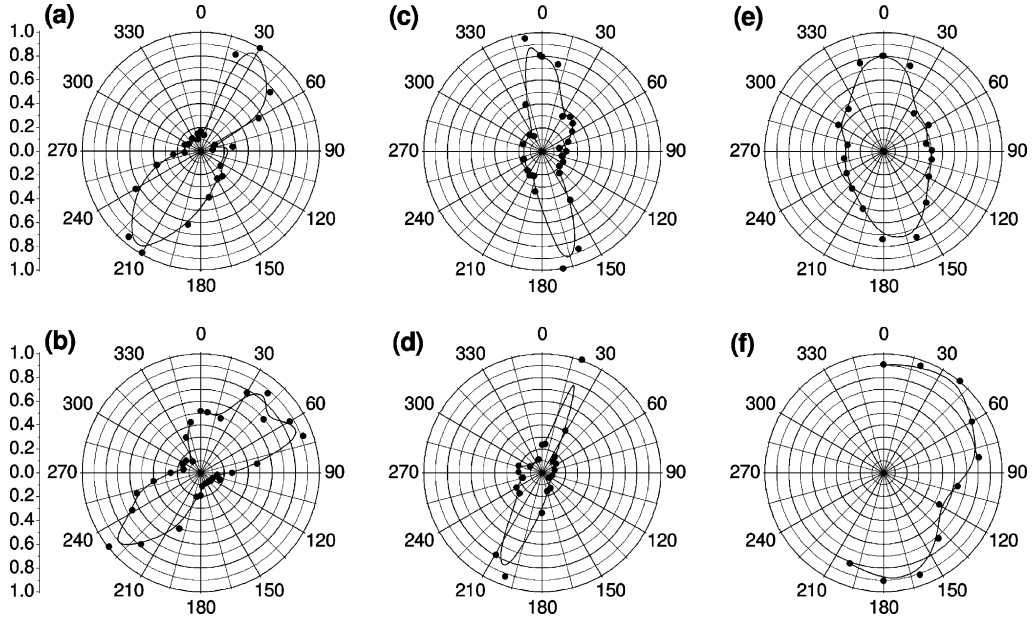

Figure 3. Polarization dependence (in polar coordinates) of $\chi^{(2)}$ susceptibility for (a) a benzylic amide macrocycle monolayer, (b) a benzylic amide macrocycle multilayer, (c) a benzylic amide [2]catenane monolayer, (d) a benzylic amide [2]catenane multilayer, (e) a fumaramide [2]rotaxane monolayer, and (f) a fumaramide [2]rotaxane multilayer, all on Ag(111).

TABLE 1: Values of the *a* Parameter [$a = \chi^{(2)}_{pp}(-2\omega;\omega,\omega)/\chi^{(2)}_{sp}(-2\omega;\omega,\omega)$] for the Studied Molecules

	macrocycle	catenane	rotaxane
multilayer	6.6	5.5	1.3
monolayer	7.2	4.8	3.0

Figure 3 displays, in polar coordinates, the dependence of the second-order nonlinear optical (NLO) susceptibility, $\chi^{(2)}$, on the angle between the fundamental and harmonic field polarizations for (a) a macrocycle monolayer, (b) a macrocycle multilayer, (c) a catenane monolayer, (d) a catenane multilayer, (e) a rotaxane monolayer, and (f) a rotaxane multilayer. As already mentioned, the harmonic beam polarization is selected to be of p-type. All susceptibilities are independently normalized to the maximum value. The sphere corresponds to $a = 1$ and the line to $a = \infty$. The width of the distribution is thus a fingerprint of the molecular order. In Table 1 we report the a parameters determined for the studied thin films. From Figure 3 and from the data in Table 1 we can see that monolayers are in general better ordered than multilayers. Among the studied compounds the highest order appears in thin films of macrocycle molecules. Due to their planar structure macrocycle molecules orient preferentially parallel to the substrate during the vacuum deposition, in agreement with previous studies.[14,18] Similar behavior is also observed for catenane, but with slightly less order. This kind of orientation was also observed in optical birefringence measurements on vacuum deposited thin films of these supramolecular structures.[19] A lesser degree of order in rotaxane thin films is not unexpected taking into account the chemical structure of these molecules.

3.2. Molecular Mechanics Studies. To explain the origin of the large SHG signal we performed theoretical calculations of the electric field experienced by the molecules on a silver surface. It is well-known that the silver surface breaks isotropy in presumably isotropic thin films deposited on it because of the large electric field created by silver atoms on the surface. The calculations were carried out for a single molecule of fumaramide [2]rotaxane deposited on Au(111) and Ag(111). The substrates were chosen for the sake of comparison. The rotaxane structure was minimized by using TINKER molecular mechanics/dynamics software package.[20−22] The Embedded Atom Model[23] was used in describing the metal−metal interactions, MM3 force field[24] for the organic−organic part, and a modified Morse potential (eq 4) in the description of metal−organic interactions

$$E(r_{ij}) = -\epsilon(1 - \{1 - \exp[-A(r_{ij} - r_0)]\}^2) \qquad (4)$$

where E is the total energy, r_{ij} the interatomic distance between atoms i and j, ϵ is well-depth, A is the Morse parameter related to the width of the well, and r_0 is the equilibrium distance between the atoms.

In addition, the charge equilibration scheme of Rappe and Goddard was applied throughout the whole system to calculate the charges used in the metal−organic Coulomb interactions.[25] This method can be used to study the evolution of partial charges when chemical environment or molecular geometry change. The metal−organic interaction model was calibrated to produce experimental desorption geometries and energies of small organic fragments consisting of similar chemical groups that can be found in rotaxane. The details of this work can be found elsewhere.[26] A metal(111) surface model consisting of five layers of 20 by 20 atoms was used and the lowest layer of metal atoms was kept fixed during the calculations. The top four layers of the surface model were allowed to relax or reconstruct to achieve the lowest energy.

The charge distribution generated by the adsorption of the rotaxane molecule on the metal(111) surface was investigated further with the Delphi4 program[27,28] to compute the electrostatic potential and the electric field on top of the surface. In Figure 4, an example of charge distribution on the Ag(111) surface is illustrated (left). The colors illustrate how the charge on the surface atoms changes as the organic adsorbs to the surface. The figure on the right shows the side view of the rotaxane on the surface along with how the charge gained from the surface atoms is distributed throughout the molecule. According to the calculations, the rotaxane orients itself on the surface in a way that one benzene ring and one carbonyl group of the thread as

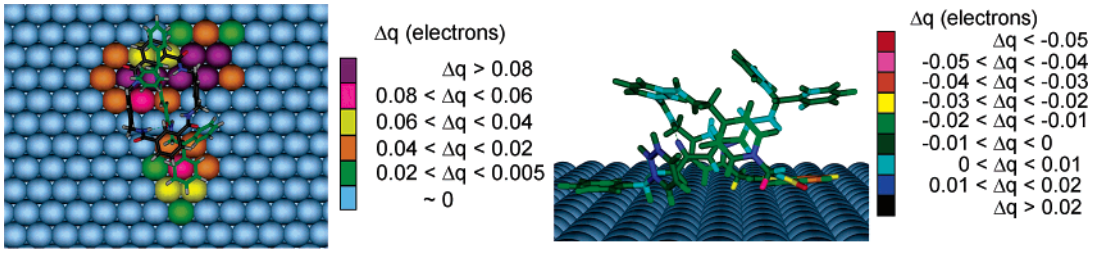

Figure 4. Left: Top view of the geometry of fumaramide [2]rotaxane on the Ag(111) surface. First layer surface atoms are colored according to their charge change. The carbon atoms in the rotaxane thread are green for clarity. Most of the positively charged atoms can be found directly below the carbonyl groups but another region of positively charged metal atoms lay below the thread benzene ring. Right: Side view of the fumaramide [2]rotaxane. The atoms are colored according to the changes in partial charges. According to the simulations the macrocycle carbonyl groups gain electron density from the silver and show the largest changes in partial charges.

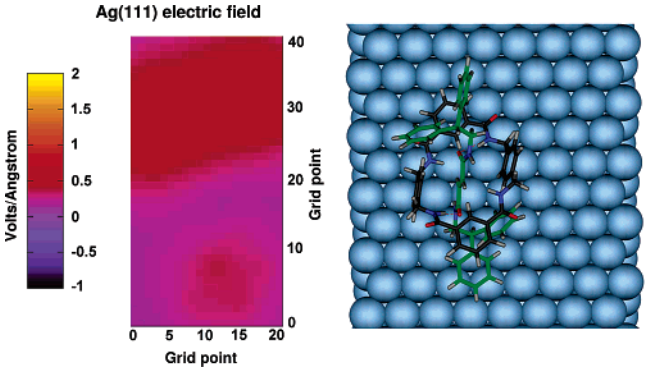

Figure 5. Left: The electric field on top of the Ag(111) surface. The distance to the surface is 1.62 Å, which corresponds to shortest surface normal of any fumaramide [2]rotaxane atom. Right: Top view of the rotaxane orientation on Ag(111).

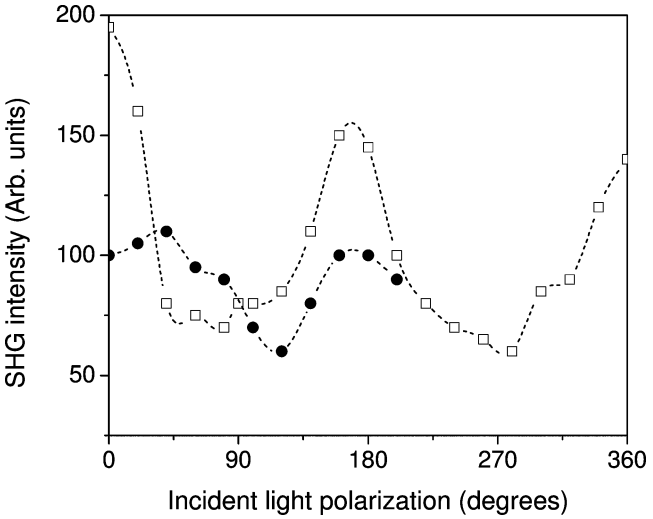

Figure 6. SHG intensity from a monolayer (□) and a multilayer (●) of fumaramide [2]rotaxane on Ag(111) as a function of the angle (in degrees) between the fundamental beam and the harmonic (fixed to be p-type) polarization directions.

well as one benzene ring and two carbonyl groups of the macrocycle are close to the surface, changing the metal charge distribution. As can be seen from Figure 4, the surface silver atoms undergo slight changes in partial charges, which are largest on atoms closest to carbonyl groups. In the beginning of the calculation, the surface is charge neutral, but as the rotaxane is adsorbed some atoms become positively charged while others obtain a small negative charge. The second group of metal atoms showing positive charges are the ones lying directly under one of the benzene rings of the thread. The additional charge density from the metal is concentrated mostly on the thread carbonyl oxygens closest to the surface and the benzene ring between them.

The electrostatic potential and the electric field were studied by using Poisson−Boltzmann algorithms in the Delphi4 program.[27,28] For this purpose, only the top layer metal atoms that had $|q| > 0.001$ electrons were considered. The charges generated on the top layer metal atoms by rotaxane adsorption were used, but the rotaxane molecule itself was excluded from the field calculations to illustrate the electric field experienced by the organic molecule when it is adsorbed to the surface. The electric field was calculated on top of the metal surface on ~17 000 evenly distributed points which were selected so that they would be inside the space occupied by the rotaxane van der Waals volume. An example of the resulting electric fields is illustrated in Figure 5. The electric field is inhomogeneous and two clearly positive areas can be distinguished. The largest positive field occurs just below the rotaxane carbonyl groups. The second and weaker field occurs below the thread benzene ring. The calculated average field strength inside the rotaxane volume of space is roughly 15 MV/cm and disappears ~9 Å away from the surface. This short depth of the electric field is confirmed by experiments. Indeed, as is seen from Figure 6 where we report the SHG intensity from a monolayer and from a multilayer of rotaxane, the two intensities are significant but the one from the multilayer is weaker.

Calculations were repeated for the rotaxane/Au(111) system and the obtained field strength was lower, about 7 MV/cm. The metal atoms in the top layer of the Au(111) surface show a larger variety of metal partial charges, but the field is weakened by the presence of negatively charged atoms, whereas in the case of Ag(111) the atoms are, on average, more positively charged.

3.3. Comparison with Experiment. Using the theoretical values of the electric field on the silver substrate, we have calculated the $\chi^{(2)}(-2\omega;\omega,\omega)$ susceptibility assuming that the SHG activity is nothing else but EFISH generation. Indeed, in previous experiments we observed only small (under pm/V) $\chi^{(2)}(-2\omega;\omega,\omega)$ susceptibilities for evaporated pristine films of catenanes and rotaxanes.[4,29] The comparison is done between the measured fumaramide [2]rotaxane thin films and the calculations for the same compound. Due to relatively complex experimental geometry the SHG intensities from rotaxane thin films were calibrated by SHG on poled polymethyl methacrylate (PMMA) thin films functionalized with disperse red #1 molecule (65:35 wt %). The poled films of this composite material were independently calibrated with SHG from an α-quartz single crystal. The value used for α-quartz for calibration is that reported in the literature by Choy and Byer[30] ($d_{11}'(-2\omega;\omega,\omega) = \chi^{(2)}_{11}(-2\omega;\omega,\omega)/2 = 0.5$ pm/V). Consequently, assuming that only the monolayer with a thickness of 9 Å contributes to the

SHG signal we obtain for $\chi^{(2)}(-2\omega;\omega,\omega)$ for the studied rotaxane a value of 23.4 pm/V.

The theoretical value derived from the electric field calculations is obtained as follows. For EFISH experiments the SHG susceptibility can be expressed as follows:

$$\chi^{(2)}(-2\omega;\omega,\omega) = NF\gamma(-2\omega;\omega,\omega,0)E \qquad (5)$$

where similarly as before, N and F are respectively the molecule density and local field factor, $\gamma(-2\omega;\omega,\omega,0)$ is EFISH molecular second hyperpolarizability, and E is the applied electric field (in this case the calculated one). Assuming $\gamma(-2\omega;\omega,\omega,0) \approx \gamma(-3\omega;\omega,\omega,\omega)$ and taking the THG values determined previously for thin films of the rotaxane under consideration ($\gamma(-3\omega;\omega,\omega,\omega) = 1.49 \times 10^{-34}$ esu) as well as the calculated electric field on the Ag surface $E = 15$ MV/cm, one obtains $\chi^{(2)}_{\mathrm{EFISH}} = 24.2$ pm/V. This is in surprisingly good agreement with the measured value, taking into account all the simplifications and approximations made. Obviously the assumption on the equality of $\gamma(-2\omega;\omega,\omega,0)$ and $\gamma(-3\omega;\omega,\omega,\omega)$ hyperpolarizabilities holds only far from the resonances, as both converge to the same value at the static ($\omega = 0$) limit. In our case we are off resonance and we may suppose that these values are not very different, although a stronger dispersion of γ_{THG} than γ_{EFISH} is expected when approaching the optical frequencies and, particularly, the absorption bands, resulting in $\gamma(-2\omega;\omega,\omega,0) \leq \gamma(-3\omega;\omega,\omega,\omega)$. Consequently the calculated EFISH values are most likely slightly overestimated.

4. Conclusions

The present study shows that catenanes and rotaxanes represent a new class of potentially interesting molecules with mobile parts for application in photonics. As with polymers, these molecules can be functionalized and their optical and physicochemical properties can be modified. Both molecules can be processed into thin film with a good optical quality. The films are characterized by optical birefringence, which is a fingerprint of molecular order. Thin films of catenane and rotaxane exhibit second harmonic generation activity. Films of the rotaxane can be poled with electric field as is the case for functionalized polymers with active NLO chromophores. Surface enhanced second harmonic generation measurements demonstrate that the highest order is found in macrocycle monolayers and the lowest, as expected, in rotaxane multilayers. Theoretical calculations show that there is a large electric field above the silver layer, which is the origin of the large SHG observed in these films. This field is a short range and disappears at a distance of about 9Å from the silver surface. We obtained remarkable agreement between the calculated and measured values.

Acknowledgment. This work was performed within the EU RT network EMMMA contract No. HPRN-CT-2002-00168 and received additional support from the EU contract MECHMOL No. IST-2001-35504, from the Dutch Foundation for Fundamental Research on Matter (FOM), and from the Breedtestrategie program of the University of Groningen.

References and Notes

(1) Sauvage, J.-P.; Dietrich-Buchecker, C., Eds. *Molecular catenanes, rotaxanes and knots*; Wiley-VCH: Weinheim, Germany, 1999.
(2) Amabilino, D. B.; Stoddart, J. F. *Chem. Rev.* **1995**, *95*, 2725.
(3) Raymo, F. M.; Stoddart, J. F. *Templated Organic Synthesis*; Wiley-VCH: Weinheim, Germany, 2000.
(4) Bermudez, V.; Gase, T.; Kajzar, F.; Capron, N.; Zerbetto, F.; Gatti, F. G.; Leigh D. A.; Zhang, S. *Opt. Mat.* **2002**, *21*, 39.
(5) Murakami, H.; Kawabuchi, A.; Kotoo, K.; Kunitake, M.; Nakashia, N. *J. Am. Chem. Soc.* **1997**, *119*, 7605.
(6) Leigh, D. A.; Wong, J. K. Y.; Dehez, F.; Zerbetto, F. *Nature* **2003**, *424*, 174.
(7) Gellert, M. *Annu. Rev. Biochem.* **1981**, *50*, 879.
(8) Wasserman, E. *J. Am. Chem. Soc.* **1960**, *82*, 4433.
(9) Johnston, A. G.; Leigh, D. A.; Pritchard, R. J.; Deegan, M. D. *Angew. Chem., Int. Ed. Engl.* **1995**, *34*, 1209.
(10) Johnston, A. G.; Leigh, D. A.; Murphy, A.; Smart, J. P.; Deegan, M. D. *J. Am. Chem. Soc.* **1996**, *118*, 10662.
(11) Johnston, A. G.; Leigh, D. A.; Nezhat, L.; Smart, J. P.; Deegan, M. D. *Angew. Chem., Int. Ed. Engl.* **1995**, *34*, 1212.
(12) Gatti, F. G.; Leigh, D. A.; Nepogodiev, S. A.; Slawin, A. M. Z.; Teat S. J.; Wong, J. K. Y. *J. Am. Chem. Soc.* **2001**, *123*, 5983.
(13) Lane, A. S.; Leigh, D. A.; Murphy, A. *J. Am. Chem. Soc.* **1997**, *119*, 11092.
(14) Whelan, C. M.; Cecchet, F.; Baxter, R.; Zerbetto, F.; Clarkson, G. J.; Leigh, D. A.; Rudolf, P. *J. Phys. Chem. B* **2002**, *106*, 8739.
(15) Fustin, C.-A.; Gouttebaron, R.; De Nadaï, C.; Caudano, R.; Rudolf, P.; Zerbetto F.; Leigh, D. A. *Surf. Sci.* **2001**, *474*, 37.
(16) Fustin, C.-A.; Rudolf, P.; Taminiaux, A. F.; Zerbetto, F.; Leigh D. A.; Caudano, R. *Thin Solid Film*s **1998**, *327*−*329*, 321.
(17) Mendoza, S. M.; Whelan, C. M.; Jalkanen, J.-P.; Zerbetto, F.; Gatti, F. G.; Kay, E. R.; Leigh, D. A.; Lubomska, M.; Rudolf, P. *J. Chem. Phys.* **2005**, *123*, 244708.
(18) Whelan, C. M.; Cechet, F.; Clarkson, G. J.; Leigh, D. A.; Caudano, R.; Rudolf, P. *Surf. Sci.* **2001**, *474*, 71.
(19) Gase, T.; Grando, D.; Chollet, P.-A.; Kajzar, F.; Lorin, A.; Leigh D. A.; Tetard, D. *Nonlinear Opt.* **1999**, *22*, 491.
(20) Ponder, J. W.; Richards, F. J. *J. Comput. Chem.* **1987**, *8*, 1016.
(21) Kundrot, C. J.; Ponder, W.; Richards, F. J. *J. Comput. Chem.* **1991**, *12*, 402.
(22) Dudek, M. J.; Ponder, J. W. *J. Comput. Chem.* **1995**, *16*, 791.
(23) Sutton, A. P.; Chen, J. *Philos. Mag. Lett.* **1990**, *61*, 139.
(24) Allinger, N. L.; Yuh, Y. H.; Lii, J.-H. *J. Am. Chem. Soc.* **1989**, *111*, 8551.
(25) Rappe, A. K.; Goddard, W. A., III *J. Phys. Chem.* **1991**, *95*, 3358.
(26) Jalkanen, J. P.; Zerbetto, F. Interaction model for the adsorption of organic molecules on the silver surfaces. *J. Phys. Chem.* In press.
(27) Rocchia, W.; Alexov, E.; Honig, B. *J. Phys. Chem. B* **2001**, *105*, 6507.
(28) Rocchia, W. S.; Sridharan, A.; Nicholls, E.; Alexov, E.; Chiabrera, A.; Honig, B. *J. Comput. Chem.* **2002**, *23*, 128.
(29) Gase, T.; Grando, D.; Chollet, P.-A.; Kajzar, F.; Murphy, A.; Leigh, D. A. *Adv. Mater*. **1999**, *11*, 1303.
(30) Choy, M.; Byer, R. L. *Phys. Rev. B* **1976**, *14*, 16993.